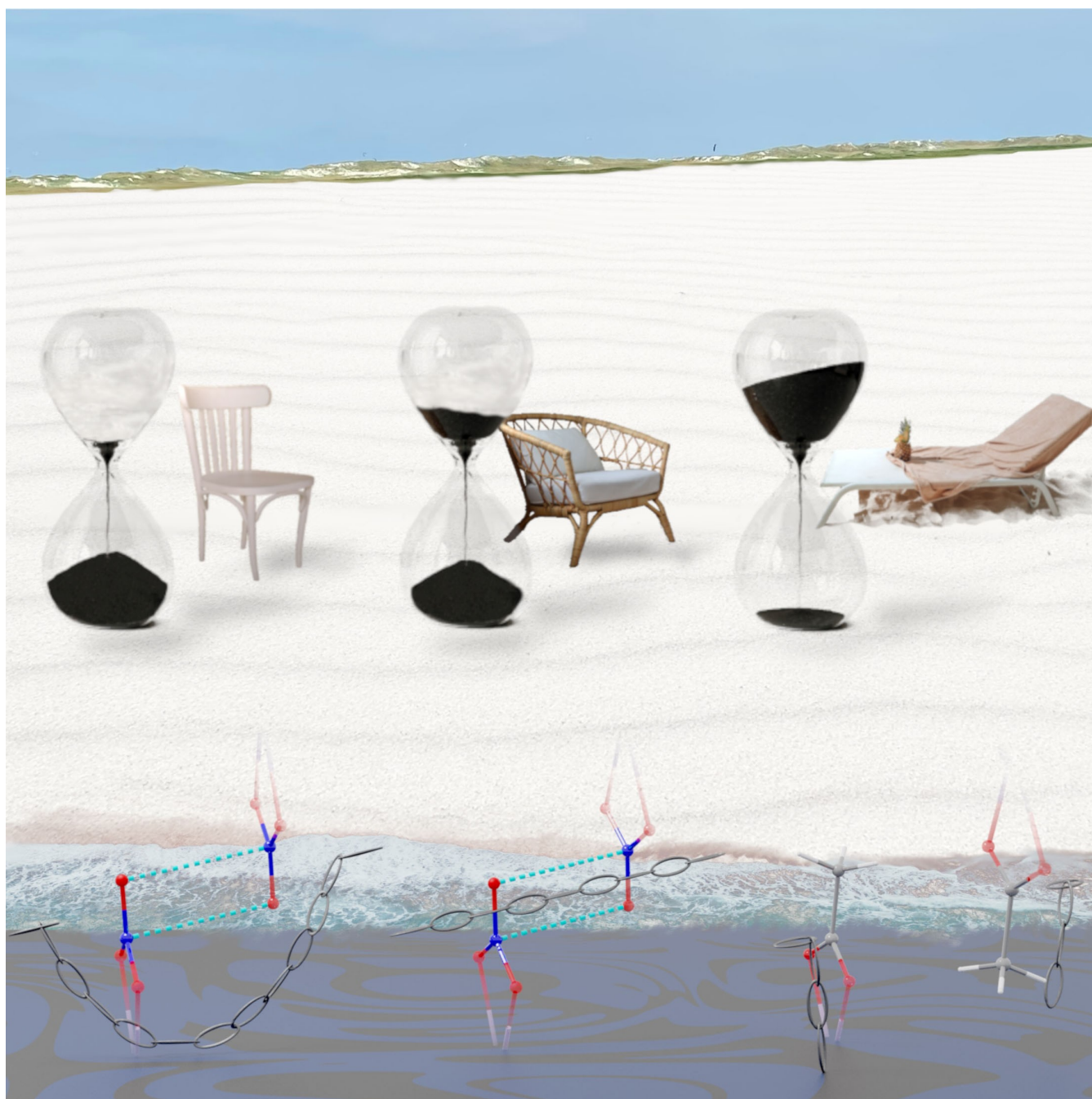


Special
Issue

Terminal Ligand and Packing Effects on Slow Relaxation in an Isostructural Set of $[\text{Dy}(\text{H}_2\text{dapp})\text{X}_2]^+$ Single Molecule Magnets**

Rouven F. Pfleger,^[a] Sören Schlittenhardt,^[b] Marcel P. Merkel,^[b] Mario Ruben,^[b, c] Karin Fink,^[b] Christopher E. Anson,^[a] Jesper Bendix,^{*,[d]} and Annie K. Powell^{*,[a, b, e]}



Abstract: We report three structurally related single ion Dy compounds using the pentadentate ligand 2,6-bis((E)-1-(2-(pyridin-2-yl)-hydrazineylidene)ethyl)pyridine (H_2dapp) [Dy(H_2dapp)(NO₃)₂NO₃ (1), [Dy(H_2dapp)(OAc)₂]Cl (2) and [Dy(H_2dapp)(NO₃)₂]Cl_{0.92}(NO₃)_{0.08} (3). The (H_2dapp) occupies a helical twisted pentagonal equatorial arrangement with two anionic ligands in the axial positions. Further influence on the electronic and magnetic structure is provided by a closely

associated counterion interacting with the central N–H group of the (H_2dapp). The slow relaxation of the magnetisation shows that the anionic acetates give the greatest slowing down of the magnetisation reversal. Further influence on the relaxation properties of compounds 1 and 2 is the presence of short nitrate-nitrate intermolecular ligand contact opening further lattice relaxation pathways.

Introduction

With the discovery of slow relaxation of the magnetisation in Ln-phthalocyanine complexes, research interest in lanthanide single ion magnets accelerated rapidly.^[1] This is due to their strong spin orbit coupling resulting in large magnetic moments and large sensitivity towards anisotropic environments. As a consequence, the ligand field largely determines the magnetic relaxation.^[2] Following the approach of engineering and optimising the electrostatic field around the lanthanide, it has proved possible to enhance the magnetic properties of molecules containing a single lanthanide ion.^[3] Single ion

complexes of Dy^{III} require ligands providing high charge density in the axial sites and low charge density in the equatorial sites. Examples with Dy^{III} derivatives of cyclopentadienyl (Cp) ligands with blocking temperatures above the boiling point of nitrogen have been reported.^[4] Comparing the structural properties of a family of systems with different substituents on the Cp rings proved not fully conclusive in terms of the role of axiality. Neither an optimisation of the 180° angle at the Dy^{III} nor reducing the distance between the ligands could be correlated with the magnetic properties.^[4b] Further investigations on the system found spin-phonon coupling responsible for the different behaviour in these systems.^[5] To date, rules on how to design compounds where the influence of phonon processes is minimised are not well-developed. This suggests that the packing of the molecules within the crystal structure could be a key to developing a better understanding of the details of structure-property relationships leading to spin-phonon relaxation phenomena. Therefore it is necessary to design systems in which small structural changes lead to fine-tuning of the magnetic properties.^[6]

For example, a dependence of the magnetic behaviour on varying solvent molecules in the lattice was found.^[7] This solvatomagnetic effect was reported to correlate with the size of the alcohol solvent molecules. Longer aliphatic chains on the molecules were shown to lead to larger energy barriers in the Orbach part of the relaxation of the magnetic moment.^[8] Furthermore, effects of different counterions on the magnetic relaxation were reported.^[9] However in the literature examples, the packing changed significantly such that different space groups were obtained with different counterions. To explore the influence of lattice properties on magnetic relaxation pathways, it is helpful to use simple systems in order to correlate the magnetic properties to changes in the crystal packing.

For this purpose, single ion complexes are ideal because influences of intramolecular interactions between spin carrying centres often responsible for reducing tunnelling processes can be excluded.^[10] Small changes in the crystal structure of larger clusters can have an effect on bond lengths to bridging atoms and influence the interactions among the magnetic centres. Furthermore, studying magnetic relaxation dynamics of single ion systems helps in assessing the contributions of 4f ions to the properties of Single Molecule Magnets (SMMs) based on two or more magnetic ions.

[a] R. F. Pflieger, Dr. C. E. Anson, Prof. Dr. A. K. Powell
Institute of Inorganic Chemistry
Karlsruhe Institute of Technology
Engesserstraße 15, 76131 Karlsruhe (Germany)
E-mail: annie.powell@kit.edu


[b] S. Schlittenhardt, Dr. M. P. Merkel, Prof. Dr. M. Ruben, Prof. Dr. K. Fink,
Prof. Dr. A. K. Powell
Institute of Nanotechnology (INT)
Karlsruhe Institute of Technology
Hermann-von-Helmholtz-Platz 1
76344 Eggenstein-Leopoldshafen (Germany)

[c] Prof. Dr. M. Ruben
Institut de Science et d'Ingénierie Supramoléculaires
(ISIS, UMR 7006)
CNRS-Université de Strasbourg
8 allée Gaspard Monge, BP 70028
67083 Strasbourg Cedex (France)


[d] Prof. J. Bendix
Department of Chemistry
University of Copenhagen
Universitetsparken 5, 2100 Copenhagen (Denmark)
E-mail: bendix@kiku.dk

[e] Prof. Dr. A. K. Powell
Institute for Quantum Materials and Technologies (IQMT)
Karlsruhe Institute of Technology
Hermann-von-Helmholtz-Platz 1
76344 Eggenstein-Leopoldshafen (Germany)

[**] H_2dapp = 2,6-bis((E)-1-(2-(pyridin-2-yl)-hydrazineylidene)ethyl)pyridine.

 Supporting information for this article is available on the WWW under <https://doi.org/10.1002/chem.202102918>

 This manuscript is part of a Special Issue "Cooperative effects in heterometallic complexes".

 © 2021 The Authors. Chemistry - A European Journal published by Wiley-VCH GmbH. This is an open access article under the terms of the Creative Commons Attribution Non-Commercial NoDerivs License, which permits use and distribution in any medium, provided the original work is properly cited, the use is non-commercial and no modifications or adaptations are made.

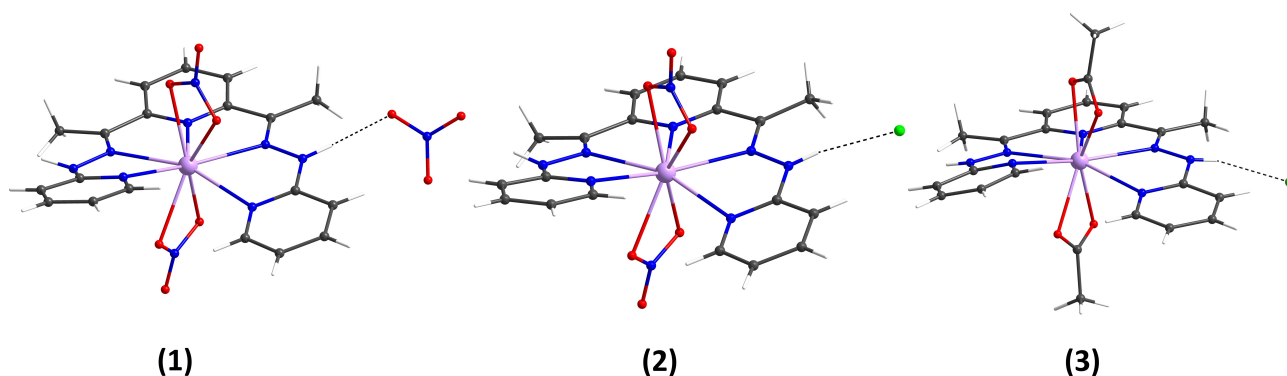


Figure 1. Molecular structure of (1), (2) and (3). Colour code: dysprosium: lilac; nitrogen: blue; oxygen: red; carbon: grey and chloride: green. The minor (8%) nitrate compositional disorder component of the counterion in (2) is omitted for clarity.

However, even single 4f ion systems show puzzling relaxation properties. So far, this has been attributed to acoustic and optical phonon mediated processes giving pathways via Raman processes. These have usually been modelled with an equation taking the Raman contribution into account in a power law resulting in exponents of 3–5 which has recently been pointed out to be inconsistent with exponents resulting from calculations^[11] on acoustic (≈ 2) and optical phonons (≈ 7 –9). On the other hand, acoustic phonon contributions should be small because of the much weaker intermolecular interactions in molecular crystals. This leads to a different density of states distribution for molecules from that expected in condensed systems. It has been suggested that the relaxation dynamics should rather be fitted with a sum of terms with exponential behaviour since this takes both the Orbach and a second order Raman process into account which are due to a first order spin-phonon coupling to the second order perturbation via a vibronic barrier.^[5b,12]

Since the coordination sphere of lanthanide ions is highly flexible, synthesising compounds with large structural similarities is not necessarily straightforward unlike the case for most 3d metal ions. Chelate ligands are helpful since they can direct the shape of the coordination sphere and direct the crystal packing. Although varying ligands to investigate the influence on the magnetic properties is well established,^[13] to our knowledge the effect on the magnetic properties of changing the counterion whilst maintaining the crystal packing at has not been systematically investigated.

Here, we report properties and structures of the three Dy^{III} complexes (1), (2) and (3) shown in Figure 1 which are structurally very similar. The Dy^{III} ion in all three complexes is chelated helically by the in situ formed pentadentate 2,6-bis((*E*)-1-(2-(pyridin-2-yl)-hydrazineylidene)ethyl)pyridine ligand (H₂dapp)^[14] in the equatorial plane and either bidentate nitrate ligands in the case of (1) and (2) or acetate ligands in the case of (3) in the axial positions. The pentadentate ligands wrap around the lanthanide ion in a helical fashion as shown in Figure 2 and as reported for some other cases.^[15]

Single crystals were obtained by stirring methanolic solutions of two equivalents of 2-hydrazinopyridine, one

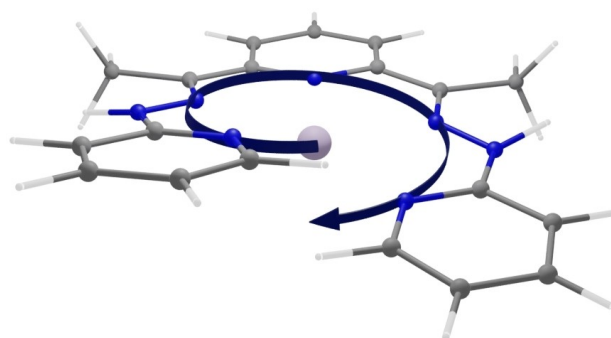


Figure 2. Helical conformation of the H₂dapp ligand.

equivalent of 2,6-diacetylpyridine and one equivalent of lanthanide salt with heating and then leaving filtered solutions to crystallise. (1) requires Dy(NO₃)₃·6H₂O, for (2) a mixture of 2/3 Dy(NO₃)₃·6H₂O and 1/3 DyCl₃·6H₂O was used and (3) was synthesised with 2/3 Dy(OAc)₃·6H₂O and 1/3 DyCl₃·6H₂O (Figure 3).

Results and Discussion

All three compounds crystallise in the space group $P\bar{1}$ with $Z = 2$. The unit cells and packing for (1) and (2) are very similar, while the packing for (3) is still related to the other two, a non-standard setting was chosen for the cell of (3) to facilitate the comparison of the packings (Supporting Information). All three complex molecules are closely isostructural with a first coordination sphere provided by the five nitrogens of the H₂dapp in the equatorial sites with the axial sites defined by two bidentate chelating nitrate ligands to give an N₅O₄ environment for (1) and (2). In the case of (3) the axial positions are taken by two chelating acetate ligands. The molecules are monocations with charge balance provided by nitrate for (1), a disordered mixture of nitrate (92%) and chloride (8%) for (2), or chloride for (3) counter anions. The density of packing is higher in (1) and (2) than in (3). This is a

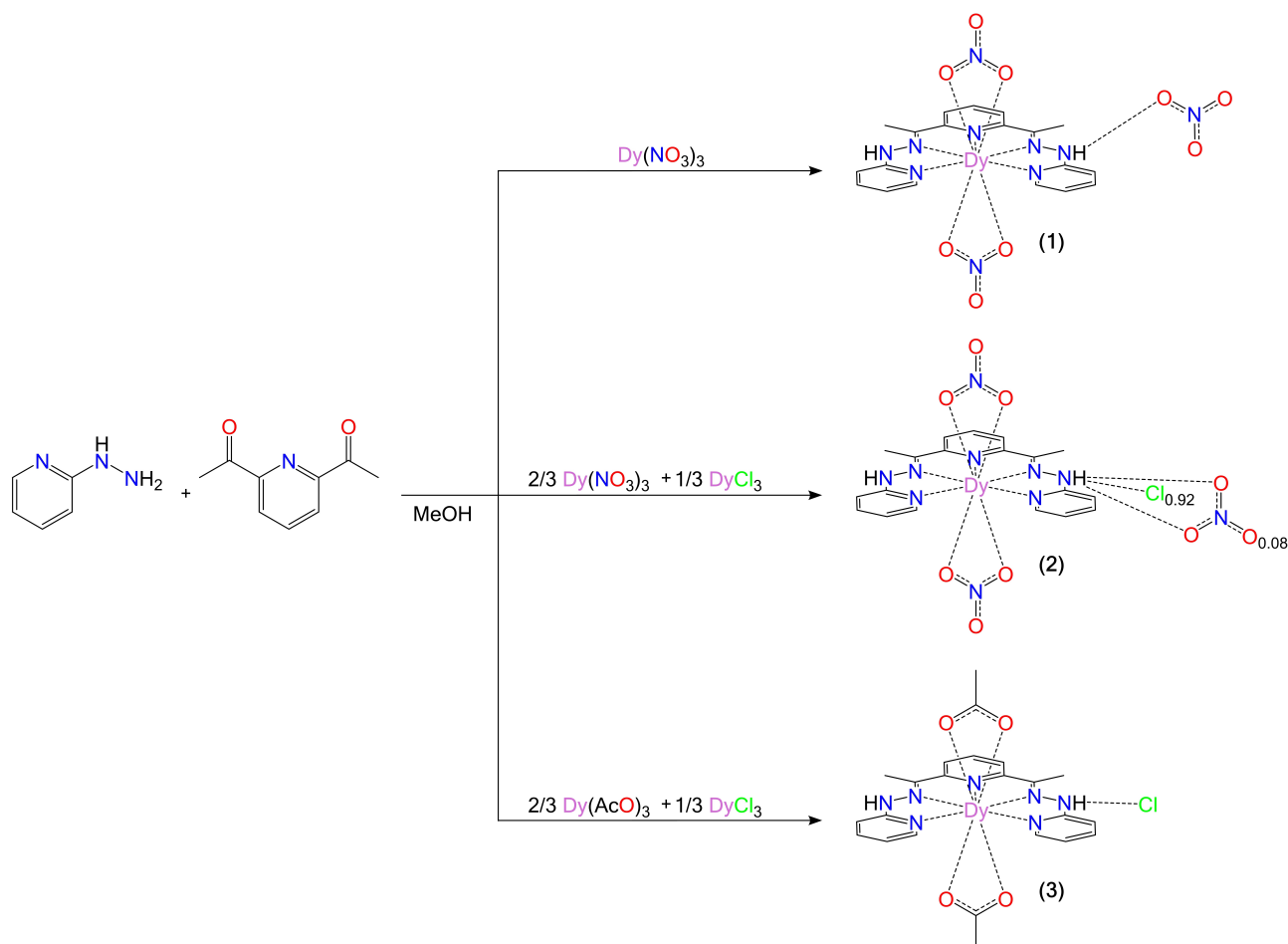


Figure 3. Reaction scheme for compound (1), (2) and (3).

result of the short nitrate-nitrate stacking as shown in Figure 4.^[16]

The short head-to-tail contact between nitrate ligands defined by the central N to the terminal non-coordinated oxygen on neighbouring molecules (Figure 4) is longer in (1) (3.031(3) Å) than in (2) (2.956(6) Å). Both these distances are less than the sum of the van der Waals radii of the nitrogen and the oxygen atoms (3.07 Å).^[17] With the spatially larger methyl groups of the acetates, this distance increases to 4.185(6) Å. Essentially these interactions hold together two molecules of opposite helicities. Between each pair there is a further packing interaction by the nitrate, chloride/nitrate, chloride counterions leading to Dy-Dy distances of 13.10 Å (1), 12.05 Å (2) and 12.80 Å (3). These are all too large to give any significant dipolar intermolecular interactions between the pairs. Since there are no solvent molecules in any of these structures the single ion properties should be conserved.

Magnetic measurements on the compounds were conducted using a Quantum Design MPMS-XL SQUID magnetometer. The room temperature χ_{MT} values are 14.28 cm³Kmol⁻¹ for (1), 14.03 cm³Kmol⁻¹ for (2) and 13.87 cm³Kmol⁻¹ for (3) which are all close to the expected value of 14.17 cm³Kmol⁻¹ for a Dy^{III} ($J = 15/2$; $g = 4/3$). In order to account for the small

deviations from the expected room temperature value these curves were normalised to this value (Figure 5). The decrease in χ_{MT} towards lower temperature of 9.97 cm³Kmol⁻¹ for (1), 10.14 cm³Kmol⁻¹ for (2) and 11.58 cm³Kmol⁻¹ for (3) is likely due to depopulation of excited M_J states. The smallest decrease found for (3) is probably due to the magnetic anisotropy of the system.

This is supported by an analysis using the MAGELLAN software and ab initio calculations.^[18] The g -tensors found for the systems can be seen in Table 1. Due to the high structural similarity of the systems, the relative anisotropy of the systems can also be estimated by comparison of the calculated reversal energies. This shows a similar anisotropy for (1) and (2) and a

Table 1. g tensors for the compounds calculated with $([\text{ML}]\text{X}_2^-)$ and without $([\text{ML}]^+)$ proximal anions.

Compound	g_x	g_y	g_z
(1)[ML] ⁺	0.25	0.56	18.61
(1)[ML]X ₂ ⁻	0.14	0.48	18.90
(2)[ML] ⁺	0.31	0.67	18.36
(2)[ML]X ₂ ⁻	0.16	0.47	18.95
(3)[ML] ⁺	0.02	0.04	19.66
(3)[ML]X ₂ ⁻	0.01	0.08	19.50

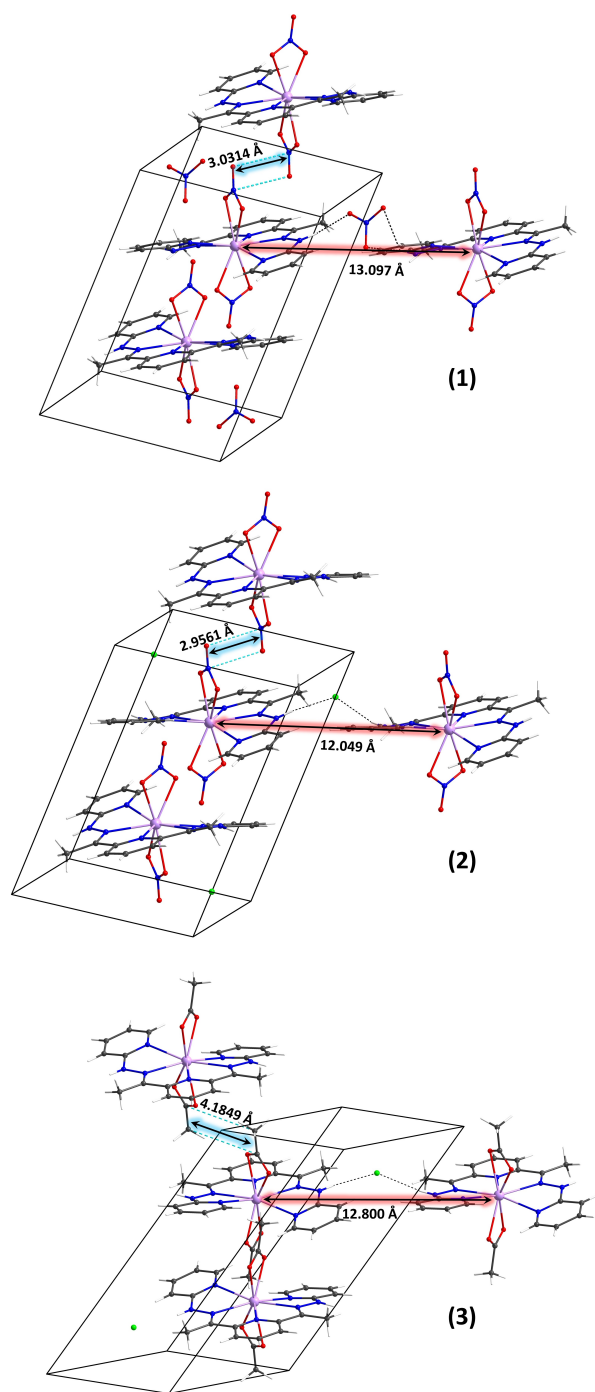


Figure 4. Intermolecular nitrate-nitrate and acetate-acetate distances in (1), (2) and (3). The minor (8%) nitrate disorder component of the counterion in (2) is omitted for clarity.

significantly larger one for (3). The small deviation in behaviour in (1) and (2) could be the result of the shorter nitrate-nitrate interaction in (2).

We calculated the relative energy levels for (1), (2) and (3) by ab initio methods without $([ML]^+)$ and with $([ML]X_2^-)$ proximal anions which create a Madelung field (Figure 6). For compounds (1) and (2) both the spacing of the Kramers doublets (KD) and the energy shifts when the Madelung field

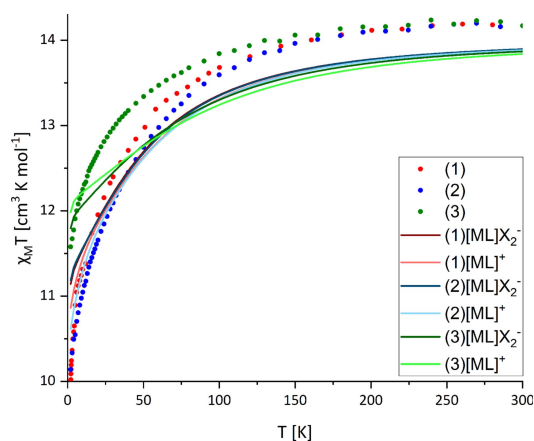


Figure 5. Measured and normalised $\chi_M T$ values for (1), (2) and (3) with fittings from ab initio calculations with $([ML]X_2^-)$ and without $([ML]^+)$ proximal anions.

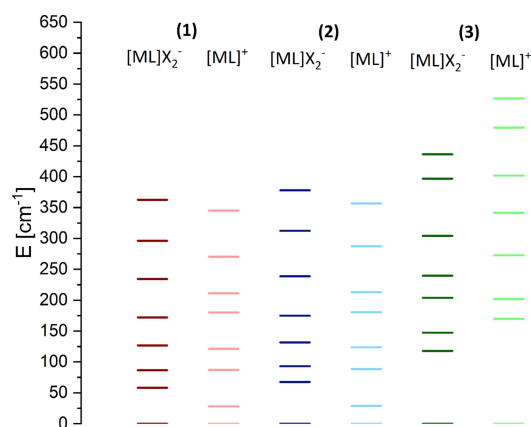


Figure 6. Energy levels from ab initio calculations for (1), (2) and (3) calculated with $([ML]X_2^-)$ and without $([ML]^+)$ proximal anions.

is taken into account are very similar. For compound (3), with its acetate ligands, the more uniaxial anisotropy as seen for the g -tensors leads to a larger splitting of the energy states particularly from the first KD to the second. In contrast to compound (1) and (2), allowing for the Madelung field decreases the gap between the first and the second KD. For compound (3) the uniaxiality is much greater with $g_z = 19.50$ than for compound (1) and (2) ($g_z = 18.90$; $g_z = 18.95$).

For all compounds it was necessary to apply a DC magnetic field in order to observe maxima for the slow relaxation in the out-of-phase AC signals within the time window of the susceptometer. This is common for the vast majority of single ion Dy complexes which often exhibit zero field quantum tunnelling of the magnetisation.^[19] The optimum fields were found to be 3000 Oe for (1), 800 Oe for (2) and 1200 Oe for (3). At this optimal DC field of 3000 Oe, there were maxima in the frequency dependent out of phase measurements detectable between 0.1 and 1 Hz up to 5 K for (1). However, an increase towards higher frequencies suggests a second maximum at higher frequencies than the measure-

ment range of 1488 Hz indicative of a second relaxation process. The data were thus fitted with a Debye model for two relaxation processes (Eqs. 1 and 2).

$$\chi'(\omega) = \chi_s + (\chi_T - \chi_s) \frac{1 + (\omega\tau)^{1-\alpha} \sin(\frac{\pi}{2}\alpha)}{1 + 2(\omega\tau)^{1-\alpha} \sin(\frac{\pi}{2}\alpha) + (\omega\tau)^{2-2\alpha}} \quad (1)$$

$$\chi''(\omega) = (\chi_T - \chi_s) \frac{(\omega\tau)^{1-\alpha} \cos(\frac{\pi}{2}\alpha)}{1 + 2(\omega\tau)^{1-\alpha} \sin(\frac{\pi}{2}\alpha) + (\omega\tau)^{2-2\alpha}} \quad (2)$$

As a result of lack of defined maxima for the second relaxation process, the extracted τ -values are of higher uncertainty for the faster relaxation process. The low frequency relaxation process is temperature-independent within the margins of error and was therefore assigned as a QTM process with a rate of 1.8 s^{-1} . For the higher frequencies, a fitting of the τ -values gave results with large error bars. However, a clear temperature-dependent trend is detectable. The temperature-dependent part could be fitted best with a Raman process with small exponent ($C=2508 \text{ s}^{-1}$; $n=2.7$). In order to compare the effects of the exchange of the counterion, (2) has been measured at the same DC field of 3000 Oe.

Also in this case, there is more than one relaxation process detectable. The slower process moved to higher frequencies of about 1 Hz while the faster process moved to smaller frequencies and maxima are detectable up to 3 K.

This means that the change of the counterion made the fastest relaxation of the system detectable up to 3 K *ceteris paribus*. From the fitting of the AC data with a Debye model for two relaxation processes, the slower relaxation consists of a temperature-dependent relaxation and a temperature-independent one visible as a shoulder in the out-of-phase susceptibility graph (Figure 7). In the $\ln(\tau)$ versus reciprocal temperature plot, this leads to an unusual shape. At lower temperatures, the temperature-dependent process is dominant and the fitted maxima belong to it. The temperature-dependent τ -values could be fitted best with a Raman process with small exponent using Equation (3) ($C=0.91 \text{ s}^{-1}$; $n=2.81$).

$$\tau(T)^{-1} = AT + B + CT^n \quad (3)$$

These small exponents in (1) and (2) need further consideration because they can only be applied if acoustic phonons can have a strong impact on the relaxation.^[12b]

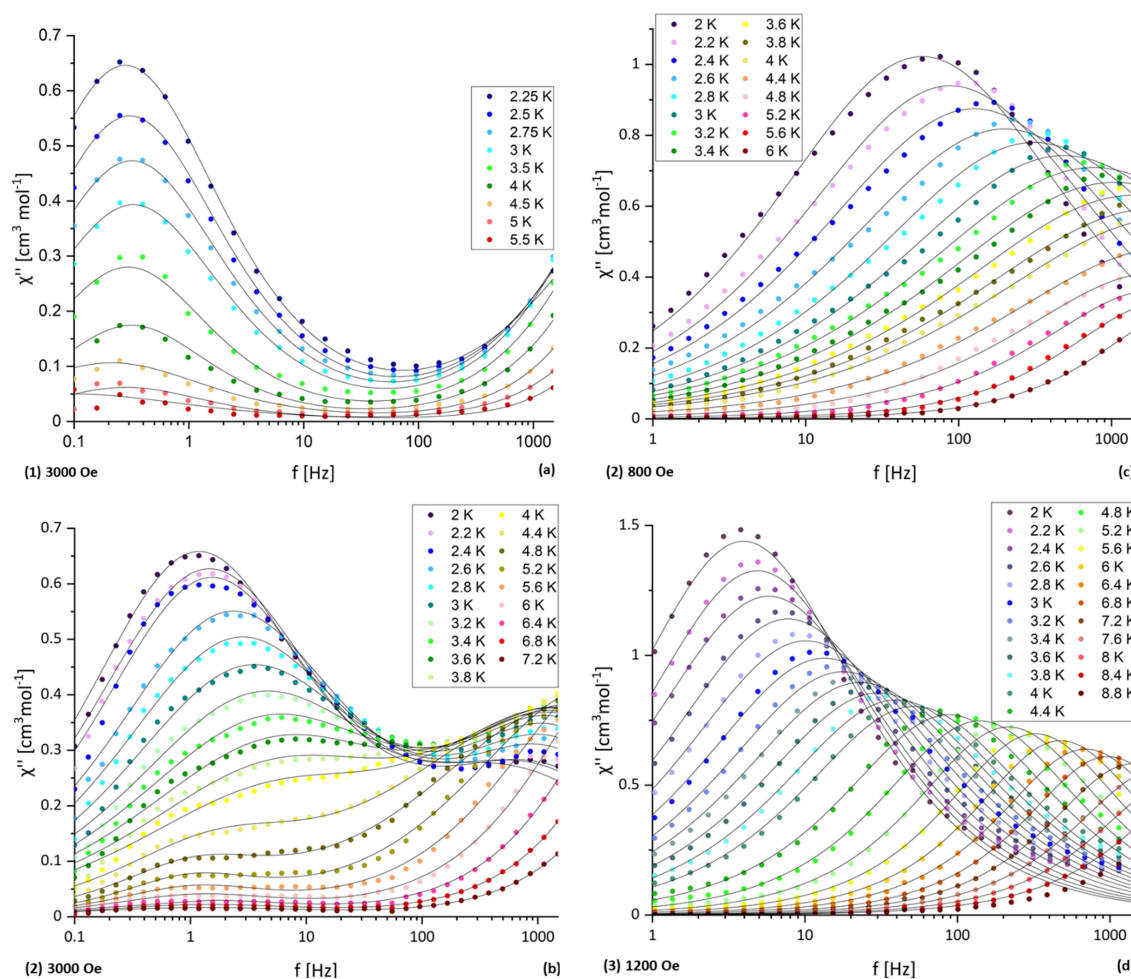


Figure 7. Out-of-phase SQUID measurements and fitting of relaxation processes (a) for (1) with 3000 Oe DC field, (b) for (2) with 3000 Oe DC field, (c) for (2) with 800 Oe DC field and (d) for (3) with 1200 Oe DC field.

Acoustic phonons are usually described as weakly coupled with the spin as they do not lead to intramolecular deformation. However, in the case of (1) and (2), acoustic phonons could have a direct impact on the intramolecular vibrations because of the nitrate-nitrate interactions. This would also explain the strong influence of the counterion on the rate (C) but the small influence on the exponent (n) as the accessibility of the process changes with the rigidity of the system. The closer packing of (2) and the better rigidity would then be responsible for the lower accessibility of the Raman process compared to (1). At higher temperatures, the temperature-independent shoulder becomes dominant. A tunnelling rate of 7.3 s^{-1} can be extracted. The presence of three relaxation processes also causes uncertainties in the fitting of the high temperature regime of the faster relaxation process. Excluding the deviating τ -values for the highest temperatures, the relaxation could be fitted in two ways following an exponential law. Firstly, according to Lunghi et al. using Equation (4) ($\omega = 20.74 \text{ K}$; $V = 840165 \text{ s}^{-1}$; $U = 72.16 \text{ K}$; $\tau_0 = 2.78 \times 10^{-10} \text{ s}$). Secondly, according to the suggestions of Gu and Wu with two equivalent exponential terms using Equation (5) ($U_a = 21.07 \text{ K}$; $\tau_{0a} = 1.09 \times 10^{-6} \text{ s}$; $U_b = 72.16 \text{ K}$; $\tau_{0b} = 2.94 \times 10^{-10} \text{ s}$).^[12a,b,d,e]

$$\tau(T)^{-1} = AT + B + V \frac{e^{\frac{\omega}{T}}}{\left(e^{\frac{\omega}{T}} - 1\right)^2} + \tau_0^{-1} e^{\frac{U}{T}} \quad (4)$$

$$\tau(T)^{-1} = AT + B + \tau_{0a}^{-1} e^{\frac{U_a}{T}} + \tau_{0b}^{-1} e^{\frac{U_b}{T}} \quad (5)$$

In both cases the exponential parameter (ω for Lunghi and Sanvito; U for Gu and Wu) represents the energy of the vibrational state responsible for the “under barrier” relaxation. The pre-exponential factors represent the rate (V for Lunghi and Sanvito; τ_0 for Gu and Wu). It should be noted that V and τ_0 are reciprocal in respect to each other.

If the DC field is turned to an optimal field of 800 Oe instead of three maxima, only one maximum at each temperature is detectable up to 3.6 K in the out-of-phase susceptibility versus frequency graph. Fitting gave $A = 141.28 \text{ s}^{-1}$; $U = 20.51 \text{ K}$ and $\tau_0 = 3.97 \times 10^{-7} \text{ s}$ using Equation (5) and $A = 142.5 \text{ s}^{-1}$; $\omega = 20.59 \text{ K}$; $V = 2525124 \text{ s}^{-1}$ using Equation (4). This suggests that moving to an optimal field, the fastest relaxation process is detectable at higher temperatures for the system.

With the change of the DC field, thermally activated quantum tunnelling appears while the faster relaxation process disappears, and the pre-exponential factor increases meaning faster relaxation via the vibrational barrier at 20.5 K or 14.24 cm^{-1} . This suggests that the quantum tunnelling is quenched at higher fields and the spin-phonon coupling increases in magnitude towards lower fields.

Under an applied optimal DC field of 1200 Oe for (3) there is only a single maximum detectable at each temperature in the out-of-phase susceptibility measurements. The maxima are visible up to 7.2 K and the data were fitted with a Debye model for one relaxation process to give the τ values at different temperatures. The relaxation was fitted with an exponential law with two terms plus in this case one term for the direct process according to Equations 4 and 5 giving $\omega = 21.67 \text{ K}$; $V = 62211 \text{ s}^{-1}$; $U = 58.65 \text{ K}$; $\tau_0 = 5.08 \times 10^{-8} \text{ s}$; $A = 12.26 \text{ s}^{-1}$ and $U_a = 21.74 \text{ K}$; $\tau_{0a} = 1.57 \times 10^{-5} \text{ s}$; $U_b = 58.03 \text{ K}$; $\tau_{0b} = 5.27 \times 10^{-8} \text{ s}$; $A = 12.27 \text{ s}^{-1}$, respectively. The ab initio calculations showed the energy splitting for compound (3) is significantly different from that in (1) and (2). The different relaxation behaviour cannot only be attributed to a different phonon density of states. However, it is remarkable that in both compounds (2) and (3) vibrational states of about 21 K or 14.6 cm^{-1} are detectable.

For a better comparison of the three systems, the relaxation time of the fastest processes in (1), (2) and (3) was plotted in a $\ln(\tau)$ versus T^{-1} graph (Figure 8) and the temperature-dependent part was fitted linearly. The fitting using Equations 4 and 5 are shown in the right part of Figure 8.

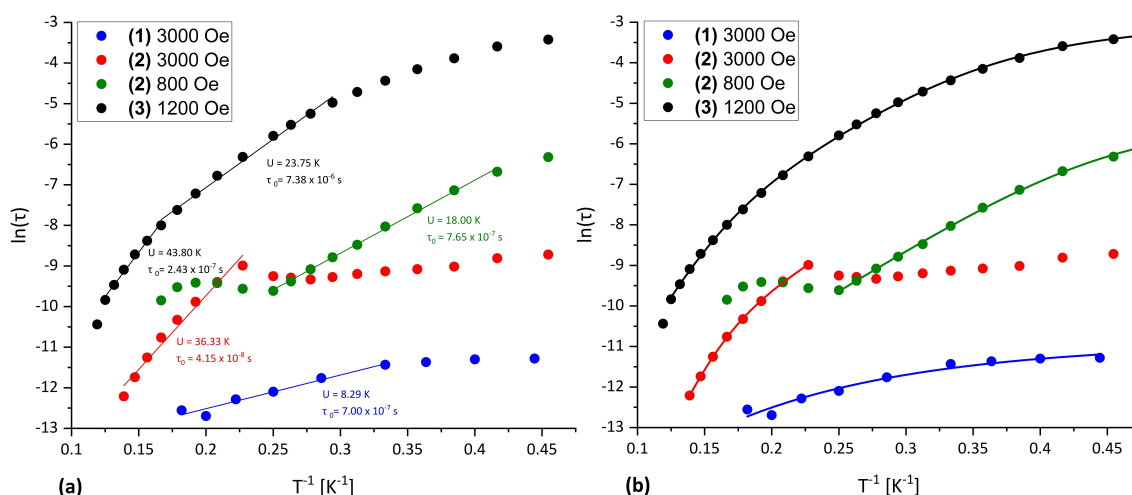


Figure 8. Relaxation properties of (1), (2) and (3) in the $\ln(\tau)$ vs. T^{-1} plot linearly fit accounting for the suggested exponential behaviour of Raman relaxations (a) and fit by the Equations 4 and 5 (b).^[12a,b,d,e]

From the linear fits, it can clearly be seen that the exchanging the nitrate counterion of (1) to the chloride in (2) leads to improved properties (increase in U and slower τ_0). Further improvement was attained by the exchange of the terminal ligands from nitrate in the case of (1) and (2) to acetate in the case of (3). That the latter is a foreseeable result becomes clear as the acetate ion can be described as the stronger base compared to the nitrate ion. Since these ions occupy axial positions in the complex, this means the acetate can provide more charge density in the axial position and stabilises the $m_J = 15/2$ ground state of the Dy^{III} .

Conclusion

Dy^{III} single ion magnets have been in general shown to be subject to various influences on the magnetic relaxation. With the isostructural Dy^{III} complexes discussed here, we have explored the effect of counterions and axial ligands under the light of two new approaches for the fitting of Raman relaxation.^[12a,b,d,e] Similar results were found using both methods. The change of nitrate to chloride counterions resulted in shorter nitrate-nitrate intermolecular distances between the axial ligands, also leading to slower relaxation of the magnetic moment. It was recently pointed out by Lunghi, Sessoli et al. that low energy optical phonons are mostly responsible for the relaxation in lanthanide SMMs.^[20] For (1) and (2) it could also be the result of opening optical phonon processes, as discussed by Gu and Wu, because of the peculiarity of the system with the π -stacking of the terminal nitrate ligands.^[12a] In order to find a clear answer to this, further investigations such as theoretical calculations on the vibrational modes and Dy nuclear resonance vibrational spectroscopy (NRVS) are needed.^[21] Furthermore, these investigations could shed light on the vibrational barrier of 14.6 cm^{-1} seen in (2) and (3). It could be clearly shown that acetate in the axial position increases the anisotropy of the system and enhances SMM properties. To provide a more detailed picture concerning the structural influences on the magnetic relaxation properties of Dy^{III} complexes, we are working on expanding this test-bed system by changing terminal ligands and exploring dinuclear systems.

Experimental Section

General procedure

All chemicals and materials were commercially available and were used without further purification. Elemental analysis (CHN) were performed on a Perkin Elmer "Vario EL". Powder X-Ray diffraction measurements were performed on a STOE STADI-P diffractometer using $Cu-K\alpha$ radiation. The data were processed using the Origin software and the simulation of powder patterns was done with Mercury 3.7. IR spectra were measured on a Bruker Alpha Platinum ATR Diamond.

Synthesis

[$Dy(H_2dapp)(NO_3)_2$] NO_3 (1)

88 mg (0.81 mmol) 2-hydrazinopyridine and 65 mg (0.4 mmol) 2,6-diacetylpyridine are dissolved in 15 ml of methanol and stirred vigorously giving a clear and pale yellow solution. A suspension of 181 mg (0.4 mmol) $Dy(NO_3)_3 \cdot 6H_2O$ and 5 ml of methanol is prepared separately and the two mixtures are combined yielding a clear but deeply coloured orange solution. The reaction mixture is heated under reflux and stirred until a precipitate forms. The slurry is filtered and the solid powder is washed with ethanol yielding [$Dy(H_2dapp)(NO_3)_2$] NO_3 . Trapezoid orange single crystals suitable for single crystal X-ray measurements are obtained by slow evaporation of the filtrate. Elemental calc. (C, H, N) 32.89%, 2.76%, 20.19%. Found 32.41%, 2.78%, 19.06%. IR/ cm^{-1} 1619 (m) 1516 (m) 1485 (m) 1422 (w) 1387 (w) 1321 (w) 1266 (s) 1192 (w) 1155 (w) 1091 (w) 1020 (w) 1003 (w) 816 (w) 780 (m) 742 (m) 488 (w) 418 (w).

[$Dy(H_2dapp)(NO_3)_2$] $Cl_{0.92}(NO_3)_{0.08}$ (2)

88 mg (0.81 mmol) 2-hydrazinopyridine and 65 mg (0.4 mmol) 2,6-diacetylpyridine are dissolved in 15 ml of methanol and stirred vigorously giving a clear and pale yellow solution. A suspension of 100 mg (0.27 mmol) $DyCl_3 \cdot 6H_2O$, 60 mg (0.13 mmol) $Dy(NO_3)_3 \cdot 6H_2O$ and 5 ml of methanol is prepared separately and the two mixtures are combined yielding a clear but deeply coloured orange solution. The reaction mixture is heated for 10 minutes at $80^\circ C$ and orange crystals of [$Dy(H_2dapp)(NO_3)_2$] $Cl_{0.92}(NO_3)_{0.08}$ are obtained suitable for single crystal X-ray measurements after leaving it for two days in a vial with porous lid. Elemental calc. (C, H, N) 34.09%, 2.86%, 19.00%. Found 33.62%, 2.86%, 17.33%. IR/ cm^{-1} 1619 (m) 1512 (m) 1483 (s) 1426 (s) 1276 (s) 1241 (m) 1192 (m) 1157 (m) 1094 (m) 1017 (s) 810 (m) 778 (s) 741 (s) 638 (s) 587 (m) 535 (m) 486 (m) 416 (m).

[$Dy(H_2dapp)(OAc)_2$] Cl (3)

88 mg (0.81 mmol) 2-hydrazinopyridine and 65 mg (0.4 mmol) 2,6-diacetylpyridine are dissolved in 15 ml of methanol and stirred vigorously giving a clear and pale yellow solution. A suspension of 100 mg (0.27 mmol) $DyCl_3 \cdot 6H_2O$, 60 mg (0.13 mmol) $Dy(OAc)_3 \cdot 6H_2O$ and 5 ml of methanol is prepared separately and the two mixtures are combined yielding a clear but deeply coloured orange solution. The reaction mixture is heated for 10 minutes at $80^\circ C$ and orange crystals of [$Dy(H_2dapp)(OAc)_2$] Cl are obtained suitable for single crystal X-ray measurements after leaving it for two days in a vial with porous lid. Elemental calc. (C, H, N) 41.76%, 3.81%, 14.82%. Found 39.99%, 3.84%, 13.66%. IR/ cm^{-1} 2930 (w,b) 1613 (m) 1522 (m) 1424 (s) 1274 (m) 1155 (s) 1093 (m) 1003 (m) 931 (w) 880 (w) 773 (s) 671 (s) 486 (m) 416 (m).

X-Ray crystallography

Datasets for the single crystal XRD measurements were measured on Bruker Apex 2 (1), Stoe STADIVARI (2) or Stoe IPDS II (3) diffractometers. For (1) and (3) $Mo-K\alpha$ ($\lambda = 0.71073\text{ \AA}$) radiation was used, while for (2) $Ga-K\alpha$ ($\lambda = 1.34143\text{ \AA}$) radiation from a MetalJet2 liquid rotating anode source was used. Structures were solved with ShelXT^[22] and refined with ShelXL^[23] within the OLEX2 platform.^[24] Non-H atoms were refined anisotropically. H atoms bonded to C were placed in calculated positions while H atoms bonded to N were refined with N–H restrained to $0.88(4)\text{ \AA}$. The counterion in (2) was found to be a disordered superposition of chloride (92%) and

nitrate (8%). The minor nitrate component was refined with geometric restraints. The conventional unit cell for (3) with $a = 9.5957(9)$, $b = 9.8276(12)$, $c = 13.5030(15)$ Å, $\alpha = 96.275(9)^\circ$, $\beta = 102.452(8)^\circ$, $\gamma = 97.565(9)^\circ$ was transformed with the matrix $\begin{bmatrix} -1 & 0 & 0 \\ 0 & -1 & 0 \\ 0 & 1 & 1 \end{bmatrix}$ to the non-conventional setting used in the refinement in order to facilitate comparisons of the packing with those of the other two compounds.

Deposition Numbers 2093949 (for (1)), 2093950 (for (2)) and 2093948 (for (3)), contain the supplementary crystallographic data for this paper. These data are provided free of charge by the joint Cambridge Crystallographic Data Centre and Fachinformationszentrum Karlsruhe Access Structures service.

Magnetic measurements

Magnetic measurements were conducted on Quantum Design MPMS-XL SQUID magnetometers with magnets capable of applying DC fields up to either 5 T or 7 T. DC susceptibility measurements were carried out under an applied field of 1000 Oe. AC measurements used an oscillating field of 3 Oe together with DC fields as described in the text. The samples were immobilised in eicosane and the data were corrected for the diamagnetic contributions of the eicosane. The sample and the sample holder based on Pascal constants.

Quantum chemical calculations

Quantum chemical calculations were performed for (1), (2) and (3) based on the experimental crystal structure. In the crystal, two of the counterions are close to the $[\text{Dy}(\text{H}_2\text{dapp})\text{X}_2]^+$. To reassemble the symmetry, the calculations were performed either for the $[\text{Dy}(\text{H}_2\text{dapp})\text{X}_2]^+$ alone (cation) or for a system including both counterions (anion). In the first step, the positions of the hydrogens were optimized at DFT level (B3-LYP functional/def2-SVP basis set/RI approximation) using TURBOMOLE^[25] for the anions with Dy replaced by Y to simplify the calculations. Starting from these structure, restricted open shell Hartree-Fock (ROHF) calculations were performed with TURBOMOLE with the x2c-TZVPall basis set^[26] with one open shell considering all sextet determinants for 9 electrons in 7f-orbitals. The respective Roothaan parameters of $a = 238/243$ and $b = 308/243$ were provided by C. van Wüllen (TU Kaiserslautern). Based on the ROHF orbitals, spin-orbit configuration interaction (SOC) calculations were performed considering all Slater determinants with 9 electrons in the 7 4f-orbitals using the CASOCI program.^[27] Scalar relativistic effects were considered using 4th order Douglas-Kroll-Hess,^[28] the two electron spin orbit contributions in a spin-orbit mean field approach.^[29] Magnetic susceptibilities were obtained by Boltzman averaging using the first eight Kramers doublets corresponding to the $J = 15/2$ ground state of the free DyIII ion. The g-values of the lowest Kramers doublet are calculated for a pseudo spin of $S = 1/2$.^[30]

Acknowledgements

We thank Dr. Olaf Fuhr for collecting single-crystal X-ray data. The presented work was supported by the Deutsche Forschungsgemeinschaft (DFG, German Research Foundation) via TRR 88 142808194 3MET, the Karlsruhe House of Young Scientists (KHYS) via the "Networking Grant" and the "Research Travel Grant" and the STN POF of the Helmholtz Foundation. Open Access funding enabled and organized by Projekt DEAL.

Conflict of Interest

The authors declare no conflict of interest.

Keywords: axiality · dysprosium · magnetic relaxation · magnetism · SMM

- [1] a) N. Ishikawa, T. Iino, Y. Kaizu, *J. Am. Chem. Soc.* **2002**, *124*, 11440–11447; b) N. Ishikawa, T. Iino, Y. Kaizu, *J. Phys. Chem. A* **2002**, *106*, 9543–9550; c) N. Ishikawa, M. Sugita, T. Ishikawa, S. Y. Koshihara, Y. Kaizu, *J. Am. Chem. Soc.* **2003**, *125*, 8694–8695; d) N. Ishikawa, M. Sugita, T. Ishikawa, S. Y. Koshihara, Y. Kaizu, *J. Phys. Chem. B* **2004**, *108*, 11265–11271.
- [2] S. G. McAdams, A.-M. Ariciu, A. K. Kostopoulos, J. P. S. Walsh, F. Tuna, *Coord. Chem. Rev.* **2017**, *346*, 216–239.
- [3] a) J. D. Rinehart, J. R. Long, *Chem. Sci.* **2011**, *2*, 2078–2085; b) L. Ungur, L. F. Chibotaru, *Phys. Chem. Chem. Phys.* **2011**, *13*, 20086–20090.
- [4] a) C. A. P. Goodwin, F. Ortu, D. Reta, N. F. Chilton, D. P. Mills, *Nature* **2017**, *548*, 439–442; b) K. R. McClain, C. A. Gould, K. Chakarawet, S. J. Teat, T. J. Groshens, J. R. Long, B. G. Harvey, *Chem. Sci.* **2018**, *9*, 8492–8503; c) F.-S. Guo, B. M. Day, Y.-C. Chen, M.-L. Tong, A. Mansikkamäki, R. A. Layfield, *Science* **2018**, *362*, 1400–1403.
- [5] a) L. Escalera-Moreno, J. J. Baldoví, A. Gaita-Ariño, E. Coronado, *Chem. Sci.* **2018**, *9*, 3265–3275; b) A. Chiesa, F. Cugini, R. Hussain, E. Macaluso, G. Allodi, E. Garlatti, M. Giansiracusa, C. A. P. Goodwin, F. Ortu, D. Reta, J. M. Skelton, T. Guidi, P. Santini, M. Solzi, R. De Renzi, D. P. Mills, N. F. Chilton, S. Carretta, *Phys. Rev. B* **2020**, *101*, 174402.
- [6] M. J. Giansiracusa, A. K. Kostopoulos, D. Collison, R. E. P. Winpenny, N. F. Chilton, *Chem. Commun.* **2019**, *55*, 7025–7028.
- [7] M. Liberka, K. Boidachenko, J. J. Zakrzewski, M. Zychowicz, J. Wang, S.-i. Ohkoshi, S. Chozazy, *Magnetochemistry* **2021**, *7*, 79.
- [8] C.-M. Liu, D.-Q. Zhang, D.-B. Zhu, *Sci. Rep.* **2017**, *7*, 15483.
- [9] a) A. B. Canaj, S. Dey, E. R. Martí, C. Wilson, G. Rajaraman, M. Murrie, *Angew. Chem. Int. Ed.* **2019**, *58*, 14146–14151; *Angew. Chem.* **2019**, *131*, 14284–14289; b) M. A. Sørensen, U. B. Hansen, M. Perfetti, K. S. Pedersen, E. Bartolomé, G. G. Simeoni, H. Mutka, S. Rols, M. Jeong, I. Zivkovic, M. Retuerto, A. Arauzo, J. Bartolomé, S. Piligkos, H. Weihe, L. H. Doerr, J. van Slageren, H. M. Rønnow, K. Lefmann, J. Bendix, *Nat. Commun.* **2018**, *9*, 1292.
- [10] Y. Peng, A. K. Powell, *Coord. Chem. Rev.* **2021**, *426*, 213490.
- [11] K. N. Shrivastava, *Phys. Status Solidi B* **1983**, *117*, 437–458.
- [12] a) L. Gu, R. Wu, *Phys. Rev. Lett.* **2020**, *125*, 117203; b) L. Gu, R. Wu, *Phys. Rev. B* **2021**, *103*, 14401; c) F. Donati, S. Rusponi, S. Stepanow, L. Persichetti, A. Singha, D. M. Juraschek, C. Wäckerlin, R. Baltic, M. Pivetta, K. Diller, C. Nistor, J. Dreiser, K. Kummer, E. Velez-Fort, N. A. Spaldin, H. Brune, P. Gambardella, *Phys. Rev. Lett.* **2020**, *124*, 77204; d) A. Lunghi, S. Sanvito, *J. Phys. Chem. Lett.* **2020**, *11*, 6273–6278; e) A. Lunghi, S. Sanvito, *J. Chem. Phys.* **2020**, *153*, 174113.
- [13] a) V. Mereacre, A. Baniodeh, C. E. Anson, A. K. Powell, *J. Am. Chem. Soc.* **2011**, *133*, 15335–15337; b) I. A. Kühne, C. E. Anson, A. K. Powell, *Front. Chem.* **2020**, *8*, 701; c) L. J. Batchelor, I. Cimatti, R. Guillot, F. Tuna, W. Wernsdorfer, L. Ungur, L. F. Chibotaru, V. E. Campbell, T. Mallah, *Dalton Trans.* **2014**, *43*, 12146–12149.
- [14] a) M. Sakamoto, N. Matsumoto, H. Okawa, *Bull. Chem. Soc. Jpn* **1991**, *64*, 691–693; b) J. D. Curry, M. A. Robinson, D. H. Busch, *Inorg. Chem.* **1967**, *6*, 1570–1574; c) Z.-X. Jiang, J.-L. Liu, Y.-C. Chen, J. Liu, J.-H. Jia, M.-L. Tong, *Chem. Commun.* **2016**, *52*, 6261–6264.
- [15] H. Wada, S. Ooka, D. Iwasawa, M. Hasegawa, T. Kajiwara, *Magnetochemistry* **2016**, *2*, 43.
- [16] a) T. J. Mooibroek, *CrystEngComm* **2017**, *19*, 4485–4488; b) C. C. Addison, N. Logan, S. C. Wallwork, C. D. Garner, *Q. Rev. Chem. Soc.* **1971**, *25*, 289–322.
- [17] S. Alvarez, *Dalton Trans.* **2013**, *42*, 8617–8636.
- [18] N. F. Chilton, D. Collison, E. J. L. McInnes, R. E. P. Winpenny, A. Soncini, *Nat. Commun.* **2013**, *4*, 2551–2558.
- [19] A. B. Canaj, S. Dey, C. Wilson, O. Céspedes, G. Rajaraman, M. Murrie, *Chem. Commun.* **2020**, *56*, 12037–12040.
- [20] M. Briganti, F. Santanni, L. Tesi, F. Totti, R. Sessoli, A. Lunghi, *J. Am. Chem. Soc.* **2021**, *143*, 13633–13645.
- [21] L. Scherthan, R. F. Pfeiffer, H. Auerbach, T. Hochdörffer, J. A. Wolny, W. Bi, J. Zhao, M. Y. Hu, E. E. Alp, C. E. Anson, R. Diller, A. K. Powell, V.

- Schünemann, *Angew. Chem. Int. Ed.* **2020**, *59*, 8818–8822; *Angew. Chem.* **2020**, *132*, 8902–8907.
- [22] G. Sheldrick, *Acta Crystallogr.* **2015**, *A71*, 3–8.
- [23] G. Sheldrick, *Acta Crystallogr.* **2015**, *C71*, 3–8.
- [24] O. V. Dolomanov, L. J. Bourhis, R. J. Gildea, J. A. K. Howard, H. Puschmann, *J. Appl. Crystallogr.* **2009**, *42*, 339–341.
- [25] TURBOMOLE V7.2 2017, a development of University of Karlsruhe and Forschungszentrum Karlsruhe GmbH, 1989–2007, TURBOMOLE GmbH, since 2007; available from <http://www.turbomole.com>.
- [26] P. Pollak, F. Weigend, *J. Chem. Theory Comput.* **2017**, *13*, 3696–3705.
- [27] T. Bodenstein, K. Fink, A. Heimermann, C. van Wüllen, *ChemPhysChem* **2021**, accepted (DOI: 10.1002/cphc.202100648).
- [28] M. Reiher, *WIREs Comput. Mol. Sci.* **2012**, *2*, 139–149.
- [29] a) B. A. Heß, C. M. Marian, U. Wahlgren, O. Gropen, *Chem. Phys. Lett.* **1996**, *251*, 365–371; b) F. Neese, *J. Chem. Phys.* **2005**, *122*, 034107.
- [30] M. Gerloch, R. F. McMeeking, *J. Chem. Soc. Dalton Trans.* **1975**, 443–2451.

Manuscript received: August 10, 2021
Accepted manuscript online: October 1, 2021
Version of record online: October 14, 2021